Matrix elements for the ground-state to ground-state $2\nu\beta^-\beta^-$ decay of Te isotopes in a hybrid model

D. R. Bes[1] and O. Civitarese[2]

[1]*Department of Physics, Tandar Labratory, Centro Atomico Constituyentes-Comision Nacional de Energia Atomica Avda Gral Paz 1499, 1650 Gral San Martin, Argentina and*

[2]*Department of Physics, University of La Plata, Casilla de Correo 67 1900, La Plata, Argentina*

(Received 18 August 2009; revised manuscript received 25 November 2009; published 28 January 2010)

Theoretical matrix elements, for the ground-state to ground-state two-neutrino double-β-decay mode ($2\nu\beta^-\beta^-$gs $\rightarrow$ gs) of ^{128,130}Te isotopes, are calculated within a formalism that describes interactions between neutrons in a superfluid phase and protons in a normal phase. The elementary degrees of freedom of the model are proton-pair modes and pairs of protons and quasineutrons. The calculation is basically a parameter-free one, because all relevant parameters are fixed from the phenomenology. A comparison with the available experimental data is presented.

DOI: 10.1103/PhysRevC.81.014315 PACS number(s): 23.40.−s, 26.30.Jk, 21.60.−n, 27.60.+j

I. INTRODUCTION

The ultimate achievement of nuclear double-β-decay (DBD) studies is to elucidate the nature of the neutrino [1,2]. To achieve this goal, one needs a set of reliable nuclear matrix elements [3], which proved to be tougher than previously thought [4]. In fact, about twenty years have elapsed since the first results produced by systematical theoretical attempts were published [5]. These treatments of the nuclear sector in DBD processes have started from two basically different approaches: (a) shell model calculations performed within a restricted basis [6] and (b) calculations based on the proton-neutron quasiparticle random-phase approximation [7–12]. In spite of impressive improvements, in practice shell model calculations are limited to the p-f shell and/or by the excitation energy of the states involved. In particular, Gamow-Teller (GT) matrix elements are renormalized through the presence of the GT giant resonance (GTR), which should decrease (increase) their absolute value if the energy difference between initial and final states is smaller (larger) than the energy of the GTR. Shell model calculations account only for the reduction by means of a coefficient of about 0.7–0.8, multiplying the GT matrix elements. This general reduction also prevents the conservation of the Ikeda sum rule. The proton-neutron quasiparticle random-phase approximation (pnQRPA) is based on the superfluid description of the single-particle motion (quasiparticle mean field), plus a random-phase approximation (RPA) treatment of residual proton-neutron interactions. The small size of the Hilbert space is a handicap for the validity of this approach to low- and intermediate-mass nuclei. Moreover, because GT matrix elements imply transitions between neutron and proton states belonging to the same shell, the available Hilbert space is further reduced for particles whose orbits are close to the beginning or the end of the shell. It is well known that quasiparticle mean field (BCS) treatment of a few particles is not advisable. Moreover, the backward contributions to the RPA amplitudes may display relatively strong violations of the Pauli principle.

In principle, one knows how to systematically correct these diseases by means of perturbation expansions [13–16], but such procedures become extremely cumbersome in all orders of perturbation, except for the lowest possible one. Alternatively, modifications of the RPA have been used (see Ref. [17] for a review of such modifications of the pnQRPA). However, some of these attempts are invalidated by the fact that the Ikeda sum rule is violated. One may also describe paired nucleons as phonons, which may annihilate, for instance, a closed-shell system [14]. This version of the nuclear field description is limited to nuclei in the vicinity of closed shells. It has been recently applied to study spin-isospin excitations in the region around $A = 56$ [18].

In the present article, we calculate DBD processes in Te isotopes. Although the neutrons may be reasonably described through a superfluid field approach, this is not the case for two and four protons outside the close shell $Z = 50$, as in Te and Xe nuclei, respectively. Therefore, we perform a hybrid treatment that describes protons as one- or two-pairing-phonon states while maintaining a superfluid picture for neutrons.

The article is organized as follows: The empirical information supporting the formalism we use in this work is presented in Sec. II, and the hybrid model is described in Sec. III. The results are presented and discussed in Sec. IV. Conclusions are drawn in Sec. V. Further details of the formalism and the analysis of the data, corresponding to the assumptions made in constructing the theory, are presented in the appendixes.

II. EMPIRICAL FRAMEWORK

In this section, we introduce the elementary degrees of freedom of the model, both fermionic and bosonic, and the essentials of the microscopic treatment of the pairing and GT sectors of the theory.

A. Macroscopic description

We identify the vacuum state $|0\rangle$ as the proton closed shell ($Z = 50$) and the BCS neutron vacuum (^{A}Sn). Fermion excitations are created by proton creation b^+_{km} or destruction b_{hm} operators and by neutron quasiparticle creation operators α^+_{jm}. Labels k, h, and j denote the quantum numbers specifying single-particle states for the magnetic quantum number m. Proton k (h) states lie above (below) the Fermi energy.

Boson excitations belong to two different types:

(i) Rotations in gauge space: There is a rotational band made up from the ground states of even Sn isotopes with the same proton closed-shell configuration.
(ii) Vibrations: Pairs of protons give rise to a vibrational pattern made by adding addition and removal phonons.

This description assumes independence between neutron and proton motions, which is certainly not exactly verified. For instance, the single-proton levels $k = d_{5/2}, g_{7/2}$ exchange positions as the neutron number N increases. Nevertheless, there is also evidence (see Appendix A) favoring the zeroth-order description introduced previously.

The proton-neutron interaction manifests itself through proton-neutron excitations (GT bosons) and the associated ground-state correlations. These modes are excited and de-excited in the $2\nu\beta^-\beta^-$ process studied here, as we discuss next.

B. Microscopic treatment

The Hamiltonian of the model includes the following sectors: (a) neutron-neutron, (b) proton-proton, and (c) proton-neutron interactions. The usual neutron-neutron interaction is written

$$H_n = -g_n P_n^+ P_n, \tag{1}$$

where the operator P_n^+ is

$$P_n^+ = \sum_j \hat{j}[c_j^+ c_j^+]^0 \tag{2}$$

(with $\hat{j} = \sqrt{j+1/2}$). The operators c_{jm}^+ are the single-neutron creation operators, which are transformed to quasineutron operators α_{jm}^+ and α_{jm} by means of the usual Bogoliubov transformation:

$$c_{jm}^+ = U_j \alpha_{jm}^+ - V_j(-1)^{j+m}\alpha_{j\bar{m}}. \tag{3}$$

The resulting quasiparticle orbits have quasiparticle energies E_j and occupation amplitudes U_j and V_j.

The proton-proton operator has the form

$$P_p^+ = \sum_k \hat{k}[b_k^+ b_k^+]^0 + \sum_h \hat{h}[b_h^+ b_h^+]^0, \tag{4}$$

and the pairing interaction is written as

$$H_p = -g_p P_p^+ P_p. \tag{5}$$

This interaction is treated within the RPA. In particular, we are interested in the properties of the Γ_0^+ boson, which is the lowest pairing addition phonon. Its energy and coupling strength are denoted by ω_0 and Λ_0, respectively (see Appendix B).

To treat the proton-neutron system, we start by defining the isoscalar pairing and GT operators. We denote by $P_{\nu q}^+$ the pair-creation operator ($\nu = 1$) and the pair-annihilation operator ($\nu = \bar{1}$),[1] both carrying the isospin $T = T_z = 0$ and angular momentum $I = 1$ with projection q:

$$\begin{aligned}
P_{1q}^+ &= \frac{\langle j_1||\sigma||j_2\rangle}{\sqrt{3}}\left(b_{j_1}^+ c_{j_2}^+\right)_q^1 \\
&= \frac{\langle k||\sigma||j\rangle}{\sqrt{3}}\left[U_j(b_k^+\alpha_j^+)_q^1 - V_j(b_k^+\alpha_j)_q^1\right] \\
&\quad + \frac{\langle j||\sigma||h\rangle}{\sqrt{3}}\left[-U_j\,(\alpha_j^+ b_h^+)_q^1 + V_j\,(\alpha_j b_h^+)_q^1\right], \\
P_{\bar{1}q}^+ &= (-1)^{1+q}(P_{1\bar{q}}^+)^+ = \frac{\langle j_1||\sigma||j_2\rangle}{\sqrt{3}}\left(c_{j_1} b_{j_2}\right)_q^1 \\
&= \frac{\langle j||\sigma||h\rangle}{\sqrt{3}}\left[V_j(\alpha_j^+ b_h)_q^1 + U_j\,(\alpha_j b_h)_q^1\right] \\
&\quad - \frac{\langle k||\sigma||j\rangle}{\sqrt{3}}\left[V_j(b_k\alpha_j^+)_q^1 + U_j(b_k\alpha_j)_q^1\right].
\end{aligned} \tag{6}$$

Similarly, we write the GT operators as $Q_{\nu q}$, carrying isospin $T = 1$ and increasing (decreasing) the isospin projection by one unit if $\nu = 1$ ($\nu = \bar{1}$). They also carry the angular momentum quantum numbers $1, q$:

$$\begin{aligned}
Q_{1q} &= -\frac{\langle j_1||\sigma||j_2\rangle}{\sqrt{3}}(b_{j_1}^+ c_{j_2})_q^1 \\
&= -\frac{\langle k||\sigma||j\rangle}{\sqrt{3}}\left[V_j(b_k^+\alpha_j^+)_q^1 + U_j(b_k^+\alpha_j)_q^1\right] \\
&\quad + \frac{\langle j||\sigma||h\rangle}{\sqrt{3}}\left[U_j(\alpha_j^+ b_h^+)_q^1 + V_j(\alpha_j b_h^+)_q^1\right], \\
Q_{\bar{1}q} &= (-1)^{1+q}(Q_{1\bar{q}})^+ = \frac{\langle j_1||\sigma||j_2\rangle}{\sqrt{3}}\left(c_{j_1}^+ b_{j_2}\right)_q^1 \\
&= \frac{\langle j||\sigma||h\rangle}{\sqrt{3}}\left[U_j(\alpha_j^+ b_h)_q^1 - V_j(\alpha_j b_h)_q^1\right] \\
&\quad + \frac{\langle k||\sigma||j\rangle}{\sqrt{3}}\left[V_j(\alpha_j^+ b_k)_q^1 - U_j(\alpha_j b_k)_q^1\right].
\end{aligned} \tag{7}$$

Although $P_{\nu q}^+$ and $Q_{\nu q}$ have good isospin quantum numbers, none of the four paired operators $[b_k^+\alpha_j^+]_q^1$, $[\alpha_j^+ b_h]_q^1$, $[b_k^+\alpha_j^+]_q^1$, and $[b_k\alpha_j]_q^1$ do, because of the superfluid description of neutrons. However, because both $P_{\nu q}^+$ and $Q_{\nu q}$ depend on these same operators, we must include the two associated schematic interactions in the proton-neutron Hamiltonian:

$$H_{pn} = -g_{pn}\sqrt{3}[P_1^+ P_{\bar{1}}^+]^0 - g\sqrt{3}[Q_1 Q_{\bar{1}}]^0. \tag{8}$$

This Hamiltonian is explicitly treated within the RPA in Appendix C. We denote by $\Gamma_{\nu n,q}^+$ the resulting phonon-creation operators, where ν has been defined previously, and $n = 1, 2, \ldots$ orders the phonons according to increasing values of their frequencies, $\omega_{\nu n}$. The corresponding coupling strengths are denoted by $\Lambda_{\nu n}$ and $\Xi_{\nu n}$ (see Appendix C).

A compact list of the parameters of the model follows:

(i) Proton single-particle levels: The most critical quantities are the particle-hole energy spacing at the shell closure $Z = 50$ ($e_{7/2} + e_{9/2}$), and the particle-particle spacing ($e_{5/2} - e_{7/2}$). The other active hole and particle states are obtained from the diagonalization of a Woods-Saxon (WS) plus Coulomb central potential, with the parameters given in Appendix B.

[1] A bar on top denotes a minus sign ($\bar{\nu} = -\nu$, $\bar{q} = -q$, and so on).

(ii) Neutron single-quasiparticle levels are determined from the BCS treatment of the pairing interaction (1) for $50 \leqslant N \leqslant 126$, in the single-particle orbits given by the WS well. The coupling g_n is fixed to reproduce to the observed gaps.

(iii) The amplitudes and couplings of the pairing phonons are fixed from the phenomenology (i.e., from binding and excitation energies) and from the population of states experimentally determined from data on (^{3}He,n) reactions.

(iv) The amplitudes and couplings of the GT phonons are determined from the known data on the energy of the GT resonance and from the measured ft values for allowed GT single-β decays in the nuclei of interest.

(v) The value of the coupling constant g_{pn} of Eq. (8) is obtained from the value determined empirically for the mass region $A = 58$, as explained in Appendix D.

We extract these parameters from empirical information independent of the DBD process that we want to study.

III. HYBRID FORMALISM

The initial and final states of the $2\nu\beta^-\beta^-$ process are described by one proton-pairing phonon (Te isotopes) and by two proton-pairing phonons (Xe isotopes). In both states, neutrons are assumed to be in the same vacuum BCS state.[2]

The whole process is divided into two stages. In the first one, the first electron-antineutrino pair is emitted. The nuclear factor of the associated interaction is proportional to the GT operator Q_{1q} (7). It creates an intermediate state from which, in the second stage, another GT operator acts, leading to the final state.

The intermediate state must be treated as a final (initial) state in the Nuclear Field Theory (NFT) sense [16], for the first (second) stage of the process, respectively. Thus, every pair of fermion lines should be eliminated from its graphical representation and replaced by its phonon counterpart. Therefore, the intermediate states populated (or depopulated) through the lowest order diagrams are

$$\begin{aligned} |an,q\rangle &= \Gamma_0^+\,\Gamma_{1n,q}^+\,|0\rangle, \\ |bn,q\rangle &= \frac{1}{\sqrt{2}}(\Gamma_0^+)^2\,\Gamma_{\bar{1}n,q}^+\,|0\rangle. \end{aligned} \tag{9}$$

They are represented by the diagrams shown in Fig. 1.

The lowest-order contributions representing each stage of the process are given in Fig. 2. Graphs 1–3 correspond to processes associated with the intermediate states $|an,q\rangle$, and graphs 4–6 are associated with the intermediate state $|bn,q\rangle$.

Graph 1 represents the direct creation of the GT resonance through the GT collective operator $(Q_{vq}^+)_{\rm coll}$ [see Eq. (C9) of Appendix C], whereas graphs 2 and 3 describe the annihilation of this resonance. Note that graph 3 represents a renormalization process of the fermion version of the GT operator acting in graph 2. Both diagrams are of the same order within the NFT formalism. The importance of including the renormalization diagrams has been stressed in Ref. [18] because they are essential, for instance, to preserve the Ikeda sum rule. In Fig. 2, the initial pairing phonon acts like a spectator. Its influence amounts to adding a factor of $\sqrt{2}$ to the matrix elements corresponding to graphs 2 and 3 and graphs 4 and 5. As usual, all time orderings should be included. The total contributions yield

$$\begin{aligned} \langle\Gamma_0^+\Gamma_{1n,q}^+|Q_{1q}|\Gamma_0^+\rangle &= -\Xi_{1n}/g, \\ \left\langle\frac{1}{\sqrt{2}}(\Gamma_0^+)^2|Q_{1\bar{q}}|\Gamma_0^+\Gamma_{1n,q}^+\right\rangle &= (-1)^{1+q}\sqrt{2}(A_{1n}+B_{1n}), \end{aligned} \tag{10}$$

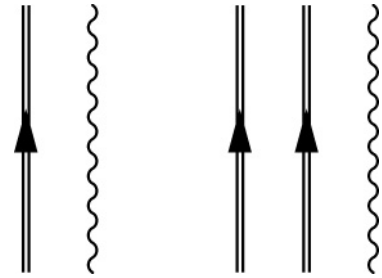

FIG. 1. Intermediate states $|an,q\rangle$ (left) and $|bn,q\rangle$ (right) of Eq. (9). Proton-proton modes are represented by a double line with an arrow, and the GT phonon is represented by a wavy line.

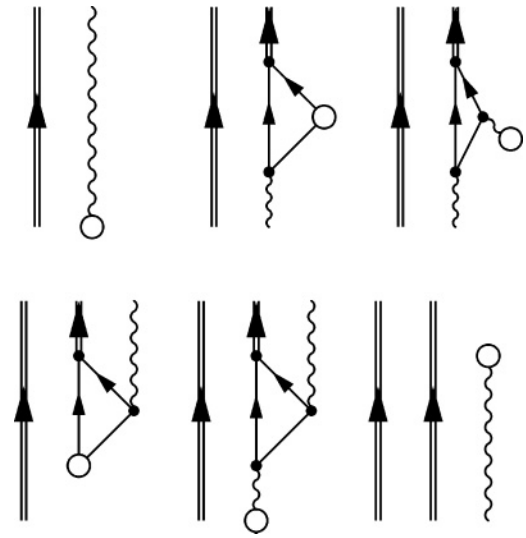

FIG. 2. Diagrams connecting the initial and final states with the intermediate states $|an,q\rangle$ [cf. Eq. (10); first row, from left to right: graphs 1–3] and with the intermediate states $|bn,q\rangle$ [cf. Eq. (12); second row, from left to right: graphs 4–6]. Open circles represent the transition operator, Q_{1q} (or $Q_{1\bar{q}}$), and the dots represent the interactions between particles and phonons. Single lines with an arrow represent proton single-particle states and bare lines represent quasineutron states.

[2]This is a reasonable assumption for systems that are sufficiently degenerate and sufficiently away from closed shells. It may be perturbatively corrected (see Chapter 7.2 of Ref. [15]). However, the corrections imply the inclusion of diagrams of an order higher than the one considered in the present work.

where

$$A_{1n} = -\frac{\Lambda_0}{3}\sum_j\left[\sum_k \frac{(\Lambda_{1n}U_j - \Xi_{1n}V_j)\langle k||\sigma||j\rangle^2}{(\omega_0 - 2e_k)(\omega_{1n} - e_k - E_j)} - \sum_h \frac{(\Lambda_{1n}U_j - \Xi_{1n}V_j)\langle j||\sigma||h\rangle^2}{(\omega_0 + 2e_h)(\omega_{1n} - \omega_0 - e_h - E_j)}\right] f_j^U(1n),$$

$$B_{1n} = \frac{\Lambda_0}{3}\sum_j\left[\sum_k \frac{(\Lambda_{1n}V_j + \Xi_{1n}U_j)\langle k||\sigma||j\rangle^2}{(\omega_0 - 2e_k)(\omega_0 - \omega_{1n} - e_k - E_j)} + \sum_h \frac{(\Lambda_{1n}V_j + \Xi_{1n}U_j)\langle j||\sigma||h\rangle^2}{(\omega_0 + 2e_h)(\omega_{1n} + e_h + E_j)}\right] f_j^V(1n). \quad (11)$$

The first stage is the more complicated one for processes associated with intermediate states $|bn, q\rangle$. It is described by graphs 4 and 5, whereas the second stage is the simple annihilation of the GT collective operator (see Appendix C). Similar considerations, as in the previous paragraph, apply here. The total contributions of these processes are given by the expressions

$$\left\langle \frac{1}{\sqrt{2}}(\Gamma_0^+)^2\Gamma^+_{\bar{1}n,q}|Q_{1q}|\Gamma_0^+\right\rangle = \sqrt{2}(A_{\bar{1}n} + B_{\bar{1}n}),$$
$$\left\langle \frac{1}{\sqrt{2}}(\Gamma_0^+)^2|Q_{1\bar{q}}|\frac{1}{\sqrt{2}}(\Gamma_0^+)^2\Gamma^+_{\bar{1}n,q}\right\rangle = (-1)^q\,\Xi_{\bar{1}n}/g, \quad (12)$$

with

$$A_{\bar{1}n} = \frac{\Lambda_0}{3}\sum_j\left[\sum_k \frac{(\Lambda_{\bar{1}n}V_j + \Xi_{\bar{1}n}U_j)\langle k||\sigma||j\rangle^2}{(\omega_0 - 2e_k)(\omega_0 + \omega_{\bar{1}n} - e_k + E_j)} - \sum_h \frac{(\Lambda_{\bar{1}n}V_j + \Xi_{\bar{1}n}U_j)\langle j||\sigma||h\rangle^2}{(\omega_0 + 2e_h)(\omega_{\bar{1}n} - e_h - E_j)}\right] f_j^V(\bar{1}n),$$

$$B_{\bar{1}n} = \frac{\Lambda_0}{3}\sum_j\left[\sum_k \frac{(\Lambda_{\bar{1}n}U_j - \Xi_{\bar{1}n}V_j)\langle k||\sigma||j\rangle^2}{(\omega_0 - 2e_k)(\omega_{\bar{1}n} + e_k + E_j)} - \sum_h \frac{(\Lambda_{\bar{1}n}V_j + \Xi_{\bar{1}n}U_j)\langle j||\sigma||h\rangle^2}{(\omega_0 + 2e_h)(\omega_0 + \omega_{\bar{1}n} - e_h - E_j)}\right] f_j^U(\bar{1}n). \quad (13)$$

The factors $f_j^{U(V)}(\nu n)$ in Refs. (11) and (13) include the renormalization contribution. They read

$$f_j^U(\nu n) = U_j - \frac{1}{g}\sum_{n'}\frac{(\Lambda_{\nu n'}V_j + \Xi_{\nu n'}U_j)\Xi_{\nu n'}}{(\nu\omega_0 - \omega_{\nu n} - \omega_{\nu n'})} - \frac{1}{g}\sum_{n'}\frac{(\Lambda_{\bar{\nu}n'}V_j + \Xi_{\bar{\nu}n'}U_j)\Xi_{\bar{\nu}n'}}{(\bar{\nu}\omega_0 + \omega_{\nu n} - \omega_{\bar{\nu}n'})},$$

$$f_j^V(\nu n) = V_j + \frac{1}{g}\sum_{n'}\frac{(\Lambda_{\nu n'}U_j - \Xi_{\nu n'}V_j)\Xi_{\nu n'}}{(\nu\omega_0 - \omega_{\nu n} - \omega_{\nu n'})} + \frac{1}{g}\sum_{n'}\frac{(\Lambda_{\bar{\nu}n'}U_j - \Xi_{\bar{\nu}n'}V_j)\Xi_{\bar{\nu}n'}}{(\bar{\nu}\omega_0 + \omega_{\nu n} - \omega_{\bar{\nu}n'})}. \quad (14)$$

IV. RESULTS AND DISCUSSIONS

To apply the previous formalism to the description of the $2\nu\beta^-\beta^-$ (gs $\rightarrow$ gs) two-neutrino DBD transition in ^{128,130}Te, we have calculated the following elementary entries:

(i) Proton single-particle energies: The single-particle and single-hole states, one shell below and one shell above the closure at $Z = 50$, that is, eleven orbits from $f_{7/2}$ to $h_{9/2}$, have been calculated with the parameters given in Eq. (B1) and in Appendix A (see Table VIII). The observables, to which we have adjusted the parameters of the standard WS plus Coulomb potential, are the intershell energy distance $e_{9/2} + e_{7/2}$ and the energy distance $e_{7/2} - e_{5/2}$, which in the present calculation yield the values 4.22 and 0.53 MeV for $A = 128$ and 4.16 and 0.58 MeV for $A = 130$, respectively. These values should be compared with the ones presented in Appendix A (see Table VIII).

(ii) Neutron quasiparticle energies: Neutron single-particle levels have been constructed, in the WS potential, with the parameters given in Eq. (20). The resulting eighteen orbits from $g_{9/2}$ to $i_{11/2}$ were treated in the BCS approximation [see Eq. (1)] with $g_n = 0.17$ MeV. The calculated gaps are of the order of $\Delta_n = 1.21$ MeV ($N = 76$) and 1.19 MeV ($N = 78$), compared with the experimentally extracted values of $\Delta_n = 1.25$ ($N = 76$) and 1.20 MeV ($N = 78$), respectively.[3] The calculated one-quasiparticle spectra, for the corresponding odd Te nuclei, assumed to be pure one-quasiparticle states, show a near degeneracy between the $h_{11/2}$ and $d_{3/2}$ states, followed by the $s_{1/2}$ state lying 1 MeV ($N = 77$) or 0.6 MeV ($N = 79$) higher, respectively.

(iii) Proton-pairing vibrations: The information about the calculated quantities is collected in Appendix B (see Table IX). For the purpose of the present calculation, we adopted the values corresponding to $b_t = 80$ MeV, that is, $g_p = 0.20$ MeV, $w_0 = 1.67$ MeV, and $\Lambda_0 = 1.003$ MeV ($A = 128$), and $g_p = 0.20$ MeV, $w_0 = 1.97$ MeV, and $\Lambda_0 = 1.00$ MeV ($A = 130$). These values are supported by the evidence of the experimental observation of features characteristic of pairing-vibrational modes collected in Appendices A and B.

(iv) Proton-neutron excitations in ^{128,130}I: The calculations have been performed in the space of proton-particle (proton-hole)–neutron–quasiparticle $I^\pi = 1^+$ configurations allowed by the states introduced in (1) and (2). We have verified that the Ikeda sum rule was fulfilled and that the calculated strength distributions, for allowed GT $0^+ \rightarrow 1^+$ transitions, shows the expected concentration of intensity around the position of the GT resonance. We found about 80% of the strength for β^- transitions in the region 10 MeV $\leqslant \omega_{1n} \leqslant$ 14 MeV and about the same quantity, 70%, for β^+ transitions in the region 6 MeV $\leqslant \omega_{\bar{1}n} \leqslant$ 8 MeV, respectively. The

[3] These values are well in agreement with the empirical mass dependence $\Delta = 11/\sqrt{A}$ MeV of Ref. [19].

TABLE I. Two-neutrino DBD of Te isotopes. The mass of the isotope is given in the first column; the second column shows the value of the half-life. The geochemical values [21,22] are given in the first two rows, and the result of the direct measurement by the NEMO collaboration for ^{130}Te [24,25] is given in the third row. Extracted experimental values of the nuclear matrix element, $M^{2\nu}_{\rm DGT}$, are shown in the last two columns for two values of g_A. The lepton phase-space integrals F_0 are scaled consistently; that is, $F_0(g_A) = (\frac{g_A}{1.254})^4 F_0(g_A = 1.254)$, and they are given in units of yrs^{-1}. The values calculated for $g_A = 1.254$ are listed in Ref. [17].

Mass	$T^{(2\nu\beta\beta)}_{1/2}$ (yrs)	Ref.	$M^{\rm exp}_{\rm DGT}$ ($g_A = 1.254$)	$M^{\rm exp}_{\rm DGT}$ ($g_A = 1.000$)
128	$2.5 \pm 0.3 10^{24}$	[21,22]	0.021 ± 0.001	0.034 ± 0.002
130	$0.9 \pm 0.1 10^{21}$	[21,22]	0.015 ± 0.001	0.023 ± 0.002
	7.6 ± 1.5 (stat.) ± 0.8 (syst.) 10^{20}	[24,25]	0.016 ± 0.002	0.027 ± 0.004

theoretical log $f_0 t$ values do compare well with the available experimental values, which are equal to 4.57 ($A = 128$) and 4.91 ($A = 130$), respectively. These values have been obtained by fixing the value of the GT coupling constant at $g = -0.14$ MeV ($A = 128$) and $g = -0.12$ MeV ($A = 130$).

In Appendix D, we discuss the scaling properties of the coupling constants used in the calculations and list their values. For completeness, the values used in the present case ($A = 128, 130$) are compared with known values extracted for the $A = 58$ mass region. The arguments presented in Appendix D are relevant, particularly to fix the value of the coupling g_{pn} of Eq. (8).

We are now in a position to calculate the nuclear matrix elements for the desired transitions in Te isotopes. As dictated by the second-order nature of the DBD transitions, we should calculate the matrix elements of the first and second stages for the same absorbed (emitted) GT phonon and sum over all GT phonons. The corresponding expression, for the allowed double-GT (DGT) matrix element, $M^{2\nu}_{\rm DGT}$, reads [17]

$$M^{2\nu}_{\rm DGT} = \sum_{i,n,q} \frac{Q_{1\bar{q}}(in) Q_{1q}(in)}{[(W_{in} + Q_{\beta\beta}/2)/(m_e c^2)] + 1}. \qquad (15)$$

The summation that appears in Eq. (15) runs on the allowed values of q and on the intermediate states belonging to the sets $|an, q\rangle$ and $|bn, q\rangle$, with energies $W_{in} = \omega_{1n}$ (if $i = a$) and $W_{in} = \omega_0 + \omega_{\bar{1}n}$ (if $i = b$), respectively. $Q_{1q}(in)$ and $Q_{1\bar{q}}(in)$ are the matrix elements given in Eqs. (10)–(12), $Q_{\beta\beta}$ is the Q value of the ground-state to ground-state DBD transition (in this case ^{128,130}Te $\rightarrow$ ^{128,130}Xe), and $m_e c^2$ is the electron mass.[4]

Current values for the half-lives of the DBD of ^{128,130}Te, obtained from geochemical determinations, are available in Refs. [20–23]. The direct measurement of the two-neutrino DBD of ^{130}Te, reported by the NEMO collaboration, can be found in Refs. [24,25]. The recommended values are displayed in Table I. The values are taken from the analysis of Barabash [24]. For the sake of completeness, in Table I, we show the values of the lepton phase-space factors, F_0, for each isotope [17]. To extract the experimental values of the nuclear matrix elements $M^{\rm exp}_{\rm DGT}$, we make use of the expression $M^{\rm exp}_{\rm DGT} = (F_0 T^{(2\nu\beta\beta)}_{1/2})^{-1/2}$. In Table I, we show the experimentally extracted values of the nuclear matrix elements $M^{\rm exp}_{\rm DGT}$, to which we include the corresponding experimental errors.

The theoretically calculated values of Ref. (15) are shown in Table II. The second column of this table shows the values obtained with $g_{pn} = 0$, and the third column gives the values of Ref. (15) corresponding to the calculation performed with this coupling fixed at the value $g_{pn} = 0.08$ MeV. Both sets of results, for $A = 128$ and $A = 130$, show the suppression of the DGT nuclear matrix elements [17]. To obtain this suppression, which is systematically present in all measured $2\nu\beta^-\beta^-$ decays [20], the use of a renormalized two-particle proton-neutron interaction was advocated long time ago [11,12] in the context of the pnQRPA formalism. As we have pointed out before, the results of pnQRPA calculations may be questioned in view of the theoretically induced isospin violations and by the failure of the BCS approach in the proximity of a shell closure. The use of the present formalism, as illustrated by the results presented in Table II, produces the observed suppression, once all the parameters involved in the calculations are fixed from data. This feature may be compared, for instance, with the adjustment procedure [17] of the conventional pnQRPA approach. We believe that this is a clear improvement of the theoretical description of the $2\nu\beta^-\beta^-$ decay in Te isotopes, actually the only DBD emitters with two protons outside the closed shell.

To illustrate the composition of the final calculated values upon the energy of the GT phonons, we show in Tables III and IV the partial contributions to the matrix element of Eq. (15).

The comparison of the results obtained with the conventional QRPA treatment and with the present hybrid formalism

TABLE II. Theoretical values of the nuclear matrix element $M^{2\nu}_{\rm DGT}$ for two values of the coupling g_{pn} of the Hamiltonian (8).

Mass	Theory ($g_{pn} = 0$)	Theory ($g_{pn} = 0.08$ MeV)
128	0.261	0.021
130	0.069	0.017

[4]Note that $M^{2\nu}_{\rm DGT}$ of Eq. (15) is dimensionless; to express it in units of inverse energy, one should divide it by the electron rest mass, $m_e c^2$. Consequently, in computing the half-life (or in extracting empirical values of the matrix element), one should use leptonic phase-space factors consistent with the adopted units.

TABLE III. Partial contributions to the DBD matrix element of Eq. (15) for the decay of ^{128}Te. Upper part of the table: the energy of the GT phonon is given in the first column. The second and third (fourth and fifth) columns give the values of the contributions coming from the summation of neutron quasiparticles and proton-particle states and neutron quasiparticles and proton-hole states of the quantity $A_{1n}(B_{1n})$ of Eq. (11). The sixth column is the partial contribution of the state ω_{1n} [including the energy denominator appearing in Eq.(15)]. The same contributions to $A_{\bar{1}n}(B_{\bar{1}n})$ of Eq. (13) are shown in the lower part of the table. The sum of the total contributions (from the upper and lower parts of the table) yields the result given in Table II.

ω_{1n} (MeV)	Term $A\ (jk)$	Term $A\ (jh)$	Term $B\ (jk)$	Term $B\ (jh)$	Partial
6.539	0.022	−0.009	0.015	−0.014	0.003
7.007	0.122	−0.032	0.017	−0.067	0.014
8.351	0.007	−0.003	0.003	−0.005	0.002
8.683	0.012	−0.010	0.003	−0.017	−0.002
8.863	0.014	−0.004	−0.005	−0.007	<0.001
9.352	0.054	−0.019	0.018	−0.032	0.008
11.152	0.028	−0.009	0.007	−0.014	0.002
12.957	0.028	−0.017	−0.019	−0.018	0.006
15.677	0.057	−0.035	0.018	−0.056	−0.008
Total					0.023
3.444	−0.015	<0.001	−0.005	−0.042	0.003
7.254	0.550	−0.283	−0.114	−1.924	−0.005
Total					−0.002

may also be illustrated by the cumulative contributions to the two-neutrino DBD [Ref. (15)]. Figure 3 shows the results for the decay of ^{128}Te, assuming the same values for the parameters entering in both calculations. As seen from these results, the fine structure of the cumulative sums differs from one method to another. They do indeed agree in the suppression obtained for $g_{pn} > 0$, but both the size and the distribution of the partial contributions are clearly different. These results may be directly confronted with data when they would become available [26]. A similar trend is observed for

TABLE IV. Partial contributions to the DBD matrix element of Eq. (15) for the decay of ^{130}Te. The meaning of the quantities is explained in the captions to Table III.

ω_{1n} (MeV)	Term $A\ (jk)$	Term $A\ (jh)$	Term $B\ (jk)$	Term $B\ (jh)$	Partial
6.720	0.037	−0.010	0.017	−0.016	0.006
7.811	<0.001	0.002	−0.007	−0.001	0.001
8.476	0.069	−0.002	0.004	−0.036	0.003
8.706	0.013	−0.004	0.001	−0.007	<0.001
9.059	0.041	−0.013	0.004	−0.020	0.003
9.699	0.044	−0.016	−0.002	−0.023	0.001
11.160	0.025	−0.010	0.011	−0.015	0.002
12.673	0.179	−0.031	−0.004	−0.062	−0.004
15.681	0.052	−0.029	0.019	−0.041	<0.001
Total					0.011
2.965	−0.025	0.001	−0.004	−0.063	0.004
7.560	−0.246	0.065	0.027	−0.689	0.002
Total					0.006

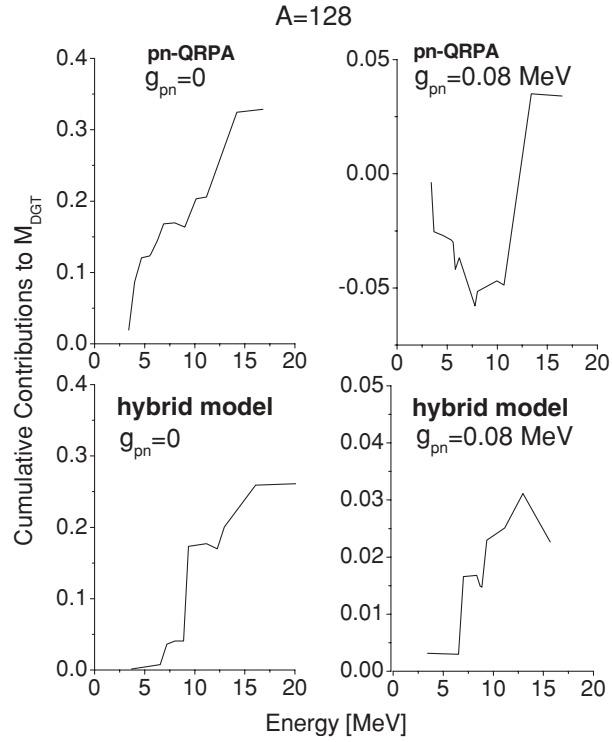

FIG. 3. Cumulative values of the matrix element in Eq. (15), as a function of the energy of the intermediate states. In the upper sector of the figure, clockwise from the left, are the contributions calculated in the conventional pnQRPA method, for $g_{pn} = 0$ and $g_{pn} = 0.08$ MeV, respectively. In the lower sector of the figure, clockwise from the left, are the contributions calculated in the hybrid model with the same values of g_{pn}. All other parameters entering in both the pnQRPA and hybrid models are the same.

the case of the system with $A = 130$. To add more information about the differences between the results of the conventional proton-neutron QRPA formalism (as we have said before, in the conventional pnQRPA approach the protons are treated in the BCS phase) and the present model (where the occupation of the proton single-particle states are given by the amplitudes of the pairing phonon, because we are treating them in the normal phase), we show in Figs. 4 and 5 the fraction of the GT transition from the ground state of Te to the excited states of I. The values correspond to the point where the matrix element of the two-neutrino mode is better reproduced in the pnQRPA (by adjusting g_{pn}) and by the hybrid model (with the parameters given in the text and in the caption to Fig. 3. Like in the case of the contributions to the matrix element of the two-neutrino mode, we see differences also here in the single-β-decay transition.

V. CONCLUSIONS

To summarize, we have presented results of the calculations of nuclear matrix elements for the two-neutrino mode of Te isotopes, which are very close to the experimentally extracted nuclear matrix elements (or to their recommended values [24]). Although similar statements of correctness, based on

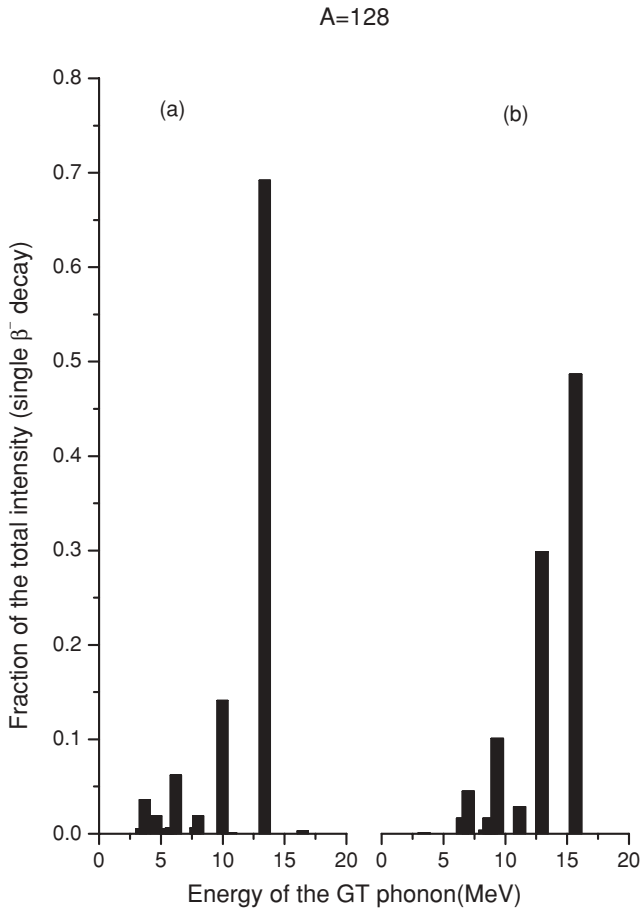

FIG. 4. Fraction of the single-β-decay intensity for the decay of ^{128}Te. Inset (a) (left-hand side of the figure) shows the results obtained with the conventional proton-neutron QRPA approximation at the point where the matrix element of the two-neutrino DBD mode is reproduced. Inset (b) (right-hand side of the figure) shows the results obtained in the present model.

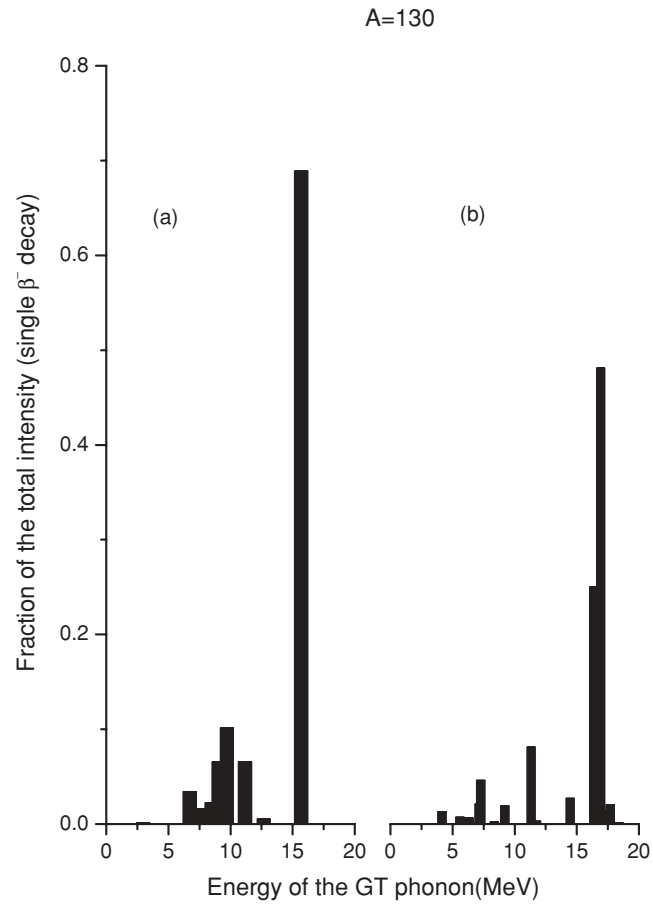

FIG. 5. Fraction of the single-β-decay intensity, for the decay of ^{130}Te, in the manner explained in the captions to Fig. 4.

the agreement with data, have been claimed by a broad spectrum of models [17], the present one exhibits some advantages:

(i) The protons are treated in a normal phase and in the isovector pairing vibrational model. This procedure is theoretically more appropriate than the standard BCS approach, which is less justified in view of the proximity of the pairing phase transition.
(ii) All parameters entering the calculations have been fixed empirically.

The present work is along the line of recently reported experimental [27] and theoretical [28] efforts to elucidate the role of pairing correlations on the matrix elements for DBD transitions. In fact, our picture can be further verified experimentally by performing additional transfer and charge-exchange reactions on Sn and Te isotopes.

Further studies are in progress concerning the calculation, within the present formalism, of nuclear matrix elements for the neutrinoless decay mode of Te isotopes, currently being measured by the NEMO and COBRA collaborations [25,29].

ACKNOWLEDGMENTS

This work has been partially supported by the National Research Council (CONICET) of Argentina, Grants PIP 5145 and PIP 112-200801-00740, and by the Agencia Nacional de Promocion Cientifica y Tecnica (ANPCYT) Grants PICT04 03-25374 and PICT07 03-00818. The authors acknowledge with pleasure the fruitful discussions with Dr. Kai Zuber (Dresden), director of the COBRA Collaboration, and with Dr. John Schiffer (Argonne). We thank Dieter Frekers (Uni-Münster) for his comments about future reaction data on Te targets.

APPENDIX A: EMPIRICAL EVIDENCE FOR THE ASSUMED COUPLING SCHEMES

Because the states that become relevant within the presently applied model belong to different nuclei, their empirical energy must be corrected by subtracting effects that are alien to the model. In particular, the volume, surface, Coulomb, and part of the isospin contributions should be eliminated. Thus, the corrected ground-state experimental energies are be given by

$$\epsilon_{A,Z}\left(\omega_{A,Z}\right) = B^{e}_{A_0,50} - B^{e}_{A,Z} - B^{w}_{A_0,50} + B^{w}_{A,Z}, \qquad \text{(A1)}$$

where $\epsilon_{A,Z}\left(\omega_{A,Z}\right)$ is used for odd (even) systems. In the case of excited states, experimental excitation energies should

be added to both sides of Ref. [16]. Here $B^e_{A,Z}$ denotes the experimental binding energy [30], and $B^w_{A,Z}$ denotes the Weizsäcker mass formula. All energies are in MeV.

$$B^w_{A,Z} = 15.5A - 17A^{2/3} - b_t T(T+1)/A - 0.7Z(Z-1)(1-0.76/Z^{2/3})/A^{1/3}. \quad \text{(A2)}$$

The strength b_t of the isospin term has been reduced from the usual value 100 MeV, because there is a contribution of the model to such term. Note that the model energies $\epsilon_{A,Z}$, $\omega_{A,Z}$ represent excitation energies relative to a vacuum state corresponding to the ground state of the ^{A_0}Sn isotope. In particular, the ground state of $^{A_0+2}$Te ($^{A_0-2}$Cd) is represented by one proton pair addition (removal) mode with frequency $\omega_a = \omega_{(A_0+2),54}(\omega_r = \omega_{(A_0-2),48})$. For the relevant cases in our calculation ($A_0 = 126, 128$), these two frequencies appear to be positive in the interval 75 MeV $< b_t <$ 90 MeV and about equal for the strength $b_t = 80$ MeV of the isospin term, which is the adopted value (see also Appendix B, Table IX and further comments, about the adopted value of the parameters).

The empirical evidence for describing the motion of neutrons in Sn isotopes as a superfluid system is well documented in the literature. The main features of this description are as follows:

(i) Nuclear masses vary smoothly but for the odd-even pairing effect. See, for instance, Figure 2.5 of Ref. [19]. The energies associated with the ground state of even superfluid systems may be grouped together in terms of rotations in gauge space. In Fig. 6, we have reinterpreted Fig. 3 of Ref. [31] using Eq. (A1). The ground-state energies of the even Sn isotopes yield the parabola

$$\omega_{A,50} = -24.188 + 0.0328\,(N - 70.640)^2 \text{ MeV}, \quad \text{(A3)}$$

with a standard deviation $\sigma = 0.14$ MeV.

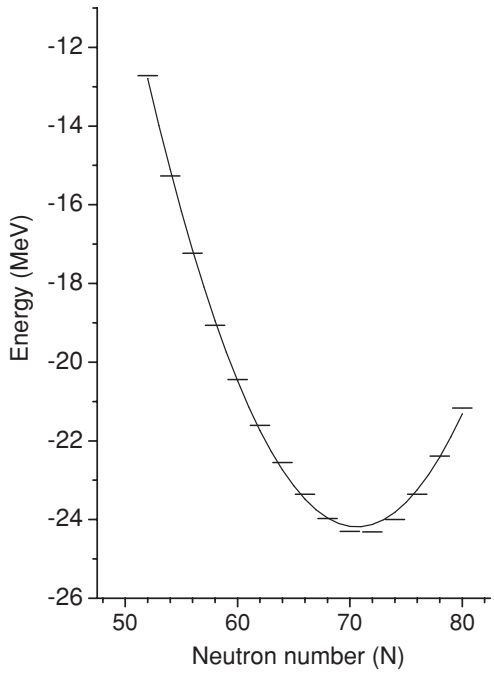

FIG. 6. The ground-state energy of even Sn isotopes, as a function of the number of neutrons N. The solid line shows the values corresponding to the (even) number of neutrons, as given by the parametrization of Eq. (A3). Horizontal lines are the experimental values.

TABLE V. Energies of the proton-pairing phonon and of the pairing vibrations as a function of the number of neutrons.

N	$\omega_{A+2,Z+2}$	$\omega_{A-2,Z-2}$	$\omega^{(pv)}_{A,Z}$	$\omega^{(\exp)}_{A,Z}$
52		1.74		
54	1.51	1.26	2.77	
56	1.49	1.10	2.59	
58	1.19	0.91	2.10	3.49
60	1.55	0.98	2.53	
62	1.36	1.11	2.47	2.88
64	1.30	1.24	2.54	2.90
66	1.41	1.26	2.67	3.02
68	1.32	1.20	2.53	2.58
70	1.30	1.21	2.51	
72	1.33	1.37	2.70	
74	1.46	1.52	2.98	
76	1.67	1.96	3.63	
78	1.94	2.33	4.27	
80	2.21	2.88	5.09	

(ii) The enhanced, specific operators for superfluid systems are the two-body transfer operators $P^+(P)$ of Eq. (2). These operators may be realized by means of (t, p) or (p, t) reactions.[5] Because fluctuations are small, the expectation value of P^+ (P) may be approximated by the gap Δ_n divided by the coupling constant g_n.

The ground-state to ground-state transitions are expected to stay fairly constant along the rotational band and to be much larger than the transitions to excited $I^\pi = 0^+$ states (see, for instance, Fig. 3 of Ref. [31]).

A vibrational coupling scheme is assumed for protons. As is well known in the case of quadrupole surface vibrations, the evidence favoring the harmonic description is generally based on the properties of the two-phonon states relative to those of one-phonon states. This model has been tested experimentally in Refs. [32–34]. The main features of the data, upon which the model has been built, are the following:

(i) Energetics: The excitation energy of the so-called pairing vibrational state in Sn nuclei (fourth column in Table V) should be given by the sum of the energies associated with addition and removal modes (second and third columns). The centroid of excited states populated through (^{3}He,n) reactions on Cd isotopes is presented in the fifth column. These centroides are obtained as weighted averages of $I^\pi = 0^+$ states populated in the interval 0–5 MeV (Table 3 of Ref. [32]). There are between two and four such states. The

[5]However, this realization is somewhat marred by the fact that in the operator associated with these reactions, j states with larger numbers of radial nodes are favored relative to Ref. (2).

TABLE VI. Energies or the two identical phonon states and their ratio with the corresponding single-phonon state as a function of the number of neutrons.

N	$\omega_{A+4,Z+4}$	$\frac{\omega_{A+4,Z+4}}{\omega_{A+2,Z+2}}$	$\omega_{A-4,Z-4}$	$\frac{\omega_{A-4,Z-4}}{\omega_{A-2,Z-2}}$
52			3.14	1.80
54			2.41	1.91
56	2.65	1.78	2.14	1.95
58	2.44	2.06	1.97	2.16
60	2.29	1.47	2.01	2.05
62	2.25	1.66	2.02	1.82
64	2.16	1.66	1.99	1.60
66	2.01	1.43	1.93	1.53
68	1.87	1.42	1.92	1.60
70	1.88	1.45	2.00	1.65
72	2.19	1.64	2.48	1.81
74	2.36	1.61	3.31	2.18
76	2.81	1.68	3.73	1.93
78	3.36	1.73		
80	3.90	1.77		
82	4.85	1.80		

agreement improves as N increases, which favors the applicability of the model in our region of interest. The ground-state energy of the $^{A+4}$Xe isotope should be twice the energy of the $^{A+2}$Te isotope. The same ratio should appear for the case of $^{A-4}$Pd and $^{A-2}$Cd isotopes (columns 4 and 5 of Table VI). Although somewhat smaller by the middle of the shell, these ratios are closer to 2, improving again for the heavier isotopes.

(ii) Population of states: Distorted wave calculations relate the experimental cross sections to the predicted ones. As in Ref. [34], we write

$$\left(\frac{d\sigma}{d\Omega}\right)_{\rm exp} = \epsilon\, C^2\, S \left(\frac{d\sigma}{d\Omega}\right)_{\rm code}, \qquad \text{(A4)}$$

where C is an isospin Clebsch-Gordan coefficient and S is the two-proton spectroscopic factor. The enhancement factor ϵ is adjusted to reproduce the data.

It is inherent to the vibrational description that the population of the pairing vibrational state of ^{A}Sn should be identical to the transition populating the ground state of $^{A+2}$Te. The second column of Table VII shows the ratio between the sum of the ϵ_i values corresponding to the population of each of the (excited) states into which the pairing vibrational state splits and the ϵ associated with the transition to the ground state of Te. The value of this ratio should be 1.

TABLE VII. Experimental ratios of the factor ϵ of Eq. (A4). The data listed in the second and third columns are taken from Ref. [32], and those in the fifth column are from Ref. [34].

N	$\frac{\sum \epsilon_i}{\epsilon(^{A}\mathrm{Te(gs)})}$	$\frac{\epsilon(^{A-4}\mathrm{Pd}\rightarrow{}^{A-2}\mathrm{Cd})}{\epsilon(^{A-2}\mathrm{Cd}\rightarrow{}^{A}\mathrm{Sn})}$	N	$\frac{\epsilon(^{A+2}\mathrm{Te}\rightarrow{}^{A+4}\mathrm{Xe})}{\epsilon(^{A}\mathrm{Sn}\rightarrow{}^{A+2}\mathrm{Te})}$
58	0.95	1.4	70	1.7
62	0.75	1.4	72	
64	0.85	1.9	74	2.1
66	1.23			
68	1.11			

Another consequence of the model is that strengths of ground-state to ground-state transitions induced by ^{3}He,n reactions should be proportional to the number of bosons in the initial state for removal phonons and to the number of bosons in the final state for addition phonons. Thus, the measured ratios listed in in the third and fifth columns of Table VII should all have the value 2. Although the experimental values are generally smaller, the situation improves again for the upper values of N.

APPENDIX B: ADOPTED VALUE OF THE PARAMETERS

1. Single-particle energies

Equations (A1) and (A2) may be also used to fix the gap between two adjacent nuclear shells. In particular, the proton single-particle distance[6] $e_{7/2} + e_{9/2}$ is obtained using the binding energies of the $^{A+1}$Sb and $^{A-1}$In isotopes. Empirical single-proton distances for the lowest excitation energy $e_{5/2} - e_{7/2}$ are taken from Ref. [35] (see Table VIII). Because these two distances are the most relevant parameters in determining the properties of the phonon Γ_0^+, an element that is crucial for our description, we have reproduce them, within a ± 50 keV tolerance, by adjusting the strengths of the spin-orbit term and the surface thickness of the WS potential (Table VIII). The remaining parameters are taken from Ref. [19]:

$$\begin{aligned} V &= -5\,\mathrm{MeV} \quad \text{protons} \\ V &= (-51 + 66\,T/A)\ \mathrm{MeV} \quad \text{neutrons} \\ V_{ls} &= -0.44\,\mathrm{V} \quad \text{neutrons} \\ R &= r_0\, A^{1/3}\ ;\ r_0 = 1.27\ \mathrm{fm} \quad \text{protons and neutrons} \\ a &= 0.67\ \mathrm{fm} \quad \text{neutrons} \end{aligned} \qquad \text{(B1)}$$

2. Properties of the lowest proton-pairing phonon Γ_0^+ and of the GT phonons

The properties of the proton-phonon are determined through the usual RPA dispersion relations. It is reassuring to verify that they are weakly dependent on the strength of the isospin term b_t in the Weizsäcker mass formula (A2). Table IX lists, as a function b_t, the addition ω_a and removal ω_r frequencies, their sum, the RPA strength Λ_0, and the strength g_p of the proton-pairing force. What matters for determining the strength is the ratio between the sums $\omega_a + \omega_r$ and twice the single-particle gap, $e_{7/2} + e_{9/2}$. This

[6]Here $e_{7/2} = \epsilon_{(A+1),51}$ and $e_{9/2} = \epsilon_{(A-1),49}$ [see Ref. (A1)].

TABLE VIII. Empirical single-proton energy distances and the adjusted WS parameters.

N	$e_{7/2} + e_{9/2}$	$e_{5/2} - e_{7/2}$	V_{ls}/V	a
76	4.18	0.491	−0.37	0.58
78	4.28	0.645	−0.37	0.58

TABLE IX. The dependence of the proton-pairing phonon Γ_0^+ on the isospin strength b_t (in units of MeV) in the Weizsäcker mass formula. This table has been constructed with the single-proton spectrum obtained with the parameters given in Eq. (B1) but for the intershell distance $(e_{7/2} + e_{9/2})$. This energy distance is obtained from Eq. (A1) as a function of the strength b_t of the isospin term (the relative distance between the upper shell levels is not changed). The energies $(\omega_a, \omega_r, e_j)$ and the couplings (Λ_0, g_0) are given in units of MeV. The factors η_j, of the last column, are the amplitudes of the pair of proton states in the $g_{7/2}$ and $d_{5/2}$ single-particle states, as they are given by the RPA treatment of protons in the pairing normal phase (see the text).

b_t	ω_a	ω_r	$(\omega_a + \omega_r)$	$(e_{7/2} + e_{9/2})$	Λ_0	g_p	$\eta_{7/2}$	$\eta_{5/2}$
70	−0.59	4.45	3.86	4.24	0.974	0.199	0.877	0.527
75	0.54	3.21	3.75	4.21	0.988	0.199	0.879	0.530
80	1.67	1.96	3.63	4.18	1.003	0.199	0.881	0.533
85	2.80	0.72	3.52	4.15	1.018	0.200	0.883	0.536
90	3.92	−0.53	3.39	4.12	1.035	0.200	0.886	0.540
95	5.05	−1.77	3.28	4.10	1.050	0.200	0.889	0.544

ratio is largely independent of the value of b_t, even for cases such that boson frequencies become negative. In the last two columns of Table IX, we have also represented the relevant amplitudes $\eta_k = -\Lambda_0 \hat{k}/(\omega_0 - 2e_k)$ $(k = g_{7/2}, d_{5/2})$, which stay practically constant over the explored range of b_t values. This verification has been performed for the case $N = 76$.

The parameters of the GT bosons, for $A = 130$, are listed in Table X. The formalism to obtain these values is explained in Appendix C.

APPENDIX C: RPA CALCULATIONS FOR THE HYBRID PROTON-NEUTRON SYSTEM

Two of the coupled operators appearing in Eqs. (6) and (7) behave as boson creation operators, namely

$$\gamma^+_{kjq} = -[b^+_k \alpha^+_j]^1_q; \quad \gamma^+_{jhq} = [\alpha^+_j b_h]^1_q. \tag{C1}$$

Therefore, the collective version of the GT operators in Eqs. (6) and (7) is given by

$$(P^+_{1q})_{\rm coll} = -\frac{\langle k||\sigma||j\rangle}{\sqrt{3}} U_j \gamma^+_{kjq} + (-1)^{1+q} \frac{\langle j||\sigma||h\rangle}{\sqrt{3}} V_j \gamma_{jh\bar{q}},$$
$$(P^+_{\bar{1}q})_{\rm coll} = \frac{\langle j||\sigma||h\rangle}{\sqrt{3}} V_j \gamma^+_{jhq} + (-1)^q \frac{\langle k||\sigma||j\rangle}{\sqrt{3}} U_j \gamma_{kj\bar{q}},$$

TABLE X. Properties of the GT bosons [see Eq. (C6)]. As an example, we show the eigenvalues and vertex functions for $A = 130$. All quantities are given in units of MeV.

n	ω_{1n}	Λ_{1n}	Ξ_{1n}	$\omega_{\bar{1}n}$	$\Lambda_{\bar{1}n}$	$\Xi_{\bar{1}n}$
1	6.720	0.029	0.101	2.965	0.246	−0.019
2	7.811	0.009	−0.069	7.560	0.163	−0.001
3	8.476	0.098	0.081			
4	8.706	0.194	0.015			
5	9.059	0.047	0.139			
6	9.699	0.056	0.174			
7	11.160	0.037	0.140			
8	12.670	0.249	−0.039			
9	15.680	0.132	0.454			

$$(Q_{1q})_{\rm coll} = \frac{\langle k||\sigma||j\rangle}{\sqrt{3}} V_j \gamma^+_{kjq} + (-1)^{1+q} \frac{\langle j||\sigma||h\rangle}{\sqrt{3}} U_j \gamma_{jh\bar{q}},$$
$$(Q_{\bar{1}q})_{\rm coll} = \frac{\langle j||\sigma||h\rangle}{\sqrt{3}} U_j \gamma^+_{jhq} + (-1)^{1+q} \frac{\langle k||\sigma||j\rangle}{\sqrt{3}} V_j \gamma_{kj\bar{q}}. \tag{C2}$$

The RPA version of the interaction (8) is given by

$$(H_{pn})_{\rm RPA} = -g_{pn}\sqrt{3}[(P^+_1)_{\rm coll}(P^+_{\bar{1}})_{\rm coll}]^0 - g\sqrt{3}[(Q_1)_{\rm coll}(Q_{\bar{1}})_{\rm coll}]^0, \tag{C3}$$

and the independent particle Hamiltonian is approximated by

$$(H_{sp})_{\rm RPA} = \epsilon_{kj}\, \gamma^+_{kjq}\gamma_{kjq} + \epsilon_{jh}\, \gamma^+_{jhq}\gamma_{jhq}, \tag{C4}$$

where $\epsilon_{kj} = e_k + E_j$, $\epsilon_{jh} = e_h + E_j$. The decoupling of the boson operators in the RPA Hamiltonian is performed as usual by means of the transformations

$$\Gamma^+_{1nq} = \lambda_{kjn}\gamma^+_{kjq} + (-1)^q \mu_{jhn}\gamma_{jh\bar{q}},$$
$$\Gamma^+_{\bar{1}nq} = \lambda_{jhn}\gamma^+_{jhq} + (-1)^q \mu_{kjn}\gamma_{kjn}. \tag{C5}$$

The linearization condition yields the frequencies $\omega_{\nu n}$ as solutions of the secular equations $\det(\omega_n) = 0$, where $\det(\omega_n)$ is the determinant of the system of equations

$$0 = \left(\frac{1}{g_p} + X_{\nu n}\right) \Lambda_{\nu n} - \nu Z_{\nu n}\, \Xi_{\nu n},$$
$$0 = -\nu Z_{\nu n}\, \Lambda_{\nu n} + \left(\frac{1}{g} + Y_{\nu n}\right) \Xi_{\nu n}, \tag{C6}$$

where

$$X_{\nu n} = -\frac{\langle k||\sigma||j\rangle^2}{3} \frac{U_j^2}{\epsilon_{kj} - \nu\omega_{\nu n}} - \frac{\langle j||\sigma||h\rangle^2}{3} \frac{V_j^2}{\epsilon_{jh} + \nu\omega_{\nu n}},$$
$$Y_{\nu n} = -\frac{\langle k||\sigma||j\rangle^2}{3} \frac{V_j^2}{\epsilon_{kj} - \nu\omega_{\nu n}} - \frac{\langle j||\sigma||h\rangle^2}{3} \frac{U_j^2}{\epsilon_{jh} + \nu\omega_{\nu n}},$$
$$Z_{\nu n} = -\frac{\langle k||\sigma||j\rangle^2}{3} \frac{\nu U_j V_j}{\epsilon_{kj} - \nu\omega_{\nu n}} + \frac{\langle j||\sigma||h\rangle^2}{3} \frac{\nu U_j V_j}{\epsilon_{jh} + \nu\omega_{\nu n}}. \tag{C7}$$

TABLE XI. Strength parameters for $A = 58$ [18] and $A = 128$. The coupling constants are given in units of MeV.

g_s	$g_s(58)$	$g_s(128)$	$\frac{g_s(128)}{g_s(58)}$
g_n	0.39	0.17	0.44
g_p	0.39	0.20	0.50
g	−0.27	−0.14	0.51
g_{pn}	0.171	0.08	0.47

The amplitudes λ and μ of Eq. (C5) are

$$\begin{aligned}
\lambda_{kjn} &= \frac{\langle k||\sigma||j\rangle}{\sqrt{3}} \frac{(\Lambda_{1n}U_j - \Xi_{1n}V_j)}{\epsilon_{kj} - \omega_{1n}}, \\
\mu_{jhn} &= -\frac{\langle j||\sigma||h\rangle}{\sqrt{3}} \frac{(\Lambda_{1n}V_j + \Xi_{1n}U_j)}{\epsilon_{jh} + \omega_{in}}, \\
\lambda_{jhn} &= -\frac{\langle j||\sigma||h\rangle}{\sqrt{3}} \frac{(\Lambda_{\bar{1}n}V_j + \Xi_{\bar{1}n}U_j)}{\epsilon_{jh} - \omega_{\bar{1}n}}, \\
\mu_{kjn} &= \frac{\langle k||\sigma||j\rangle}{\sqrt{3}} \frac{\sigma_{kj}(\Lambda_{\bar{1}n}U_j - \Xi_{\bar{1}n}V_j)}{\epsilon_{kj} + \omega_{\bar{1}n}}.
\end{aligned} \tag{C8}$$

The ratio $\Xi_{\nu n}/\Lambda_{\nu n}$ is obtained from either one of Eqs. (C6), and the absolute value of $\Lambda_{\nu n}$ is given by the normalization condition of the $\Gamma^+_{\nu n}$ operators.

Inversion of Eq. (C5) yields the final version of the collective GT operators [Eq. (C2)],

$$\begin{aligned}
(P^+_{\nu q})_{\rm coll} &= \frac{1}{g_p}[-\Lambda_{\nu n}\Gamma^+_{\nu nq} + (-1)^q \Lambda_{\bar{\nu}n}\Gamma_{\bar{\nu}n\bar{q}}], \\
(Q^+_{\nu q})_{\rm coll} &= \frac{1}{g}[-\Xi_{\nu n}\Gamma^+_{\nu nq} + (-1)^q \Xi_{\bar{\nu}n}\Gamma_{\bar{\nu}n\bar{q}}],
\end{aligned} \tag{C9}$$

TABLE XII. Neutron quasiparticle (BCS) states considered in the calculations for $A = 128$. The value of the pairing coupling constant is given in the text. The single-particle energies have been calculated as explained in the text. The numbers given in columns, from left to right, are the principal quantum number, the orbital quantum number, the angular momentum, and the quasiparticle energy, respectively.

N	l	j	v_j	u_j	E_{qp} (MeV)
6	6	5.5	0.99928	0.03799	15.82671
6	4	3.5	0.99921	0.03984	15.09468
6	2	1.5	0.99912	0.04184	14.37493
6	0	0.5	0.99903	0.04405	13.65566
6	2	2.5	0.99891	0.04662	12.90317
6	4	4.5	0.99863	0.05226	11.51384
6	6	6.5	0.99692	0.07846	7.68237
5	1	0.5	0.99662	0.08215	7.33964
5	1	1.5	0.99541	0.09573	6.30590
5	3	2.5	0.99671	0.08106	7.43704
5	5	4.5	0.99558	0.09395	6.42422
5	3	3.5	0.99087	0.13482	4.49807
5	5	5.5	0.66034	0.75097	1.21171
4	2	1.5	0.38483	0.92299	1.69171
4	0	0.5	0.29668	0.95498	2.12086
4	4	3.5	0.18448	0.98284	3.31405
4	2	2.5	0.16110	0.98694	3.77930
4	4	4.5	0.07919	0.99686	7.61155

TABLE XIII. Neutron quasiparticle (BCS) states considered in the calculations for $A = 130$. The value of the pairing coupling constant is given in the text. The single-particle energies have been calculated as explained in the text. The numbers given in columns, from left to right, are the principal quantum number, the orbital quantum number, the angular momentum, and the quasiparticle energy, respectively.

N	l	j	v_j	u_j	E_{qp} [MeV]
6	6	5.5	0.99925	0.03876	15.45957
6	4	3.5	0.99917	0.04069	14.72763
6	2	1.5	0.99908	0.04278	14.00799
6	0	0.5	0.99898	0.04510	13.28884
6	2	2.5	0.99886	0.04782	12.53651
6	4	4.5	0.99855	0.05379	11.14755
6	6	6.5	0.99662	0.08209	7.31853
5	1	0.5	0.99628	0.08615	6.97624
5	1	1.5	0.99486	0.10125	5.94430
5	3	2.5	0.99638	0.08496	7.07350
5	5	4.5	0.99506	0.09926	6.06237
5	3	3.5	0.98927	0.14607	4.14348
5	5	5.5	0.54765	0.83671	1.30670
4	2	1.5	0.32174	0.94683	1.96549
4	0	0.5	0.25472	0.96702	2.43086
4	4	3.5	0.16599	0.98613	3.65796
4	2	2.5	0.14661	0.98919	4.12852
4	4	4.5	0.07530	0.99716	7.97441

and the particle-vibration Hamiltonian vertices,

$$\begin{aligned}
H_{pv} = &-g_{pn}\sqrt{3}\{[(P^+_1)_{\rm coll}\, P^+_{\bar{1}}]^0 + [P^+_1\,(P^+_{\bar{1}})_{\rm coll}]^0\} \\
&- g\sqrt{3}\{[(Q_1)_{\rm coll}\, Q_{\bar{1}}]^0 + [Q_1\,(Q_{\bar{1}})_{\rm coll}]^0\}.
\end{aligned} \tag{C10}$$

APPENDIX D: STRENGTH OF THE ISOSCALAR PAIRING INTERACTION

A general statement can be made concerning the dependence of the strengths of different effective forces on the mass number A [36–38]. It is based on the fact that effects associated with such forces coexist with the shell model along the whole of the periodic table. The single-particle level-bunching energy is of the order of the shell spacing $\hbar\omega$ times the shell degeneracy $\mathcal{O}(A^{2/3})$:

$$\mathcal{O}(A^{-1/3}) \times \mathcal{O}(A^{2/3}) = \mathcal{O}(A^{1/3}). \tag{D1}$$

Let us repeat the argument used in Ref. [38] for the isovector pairing strength. One defines the pairing momentum as

$$\sum_\nu U_\nu V_\nu = \mathcal{O}(A^{2/3}) \times \mathcal{O}(1) = \mathcal{O}(A^{2/3}), \tag{D2}$$

where the factor of $\mathcal{O}(1)$ is a typical product $U_\nu V_\nu (\leqslant 1)$ of the factors appearing in the quasiparticle transformation [Eq. (3)]. The energy associated with the isovector pairing force is of the form

$$-g_{n(p)}\left(\sum_{lm} U_{lm}V_{lm}\right)^2 = -g_{n(p)}\,\mathcal{O}(A^{4/3}). \tag{D3}$$

Therefore, the expected dependence $A^{1/3}$ [see Eq. (D1)] of the pairing energy is consistent with the estimates

$$g_{n(p)} \propto A^{-1}. \tag{D4}$$

A similar estimate can be made in cases of the isoscalar pairing and GT interactions. The corresponding momenta can be written as in the right-hand side of Eq. (D1), with the factor of $\mathcal{O}(1)$ representing a (spin) matrix element of the Pauli operator $\vec{\sigma}$. Therefore, we also obtain

$$g_{np} \propto A^{-1}, \quad g \propto A^{-1}. \tag{D5}$$

This dependence can be verified for the isovector pairing and GT interactions through the ratio of respective strengths in the regions $A = 58$ [18] and $A = 128$ (Appendix B). These ratios are close to the number $58/128 = 0.45$. Note that the values listed in the first three rows of Table XI have been obtained independently of Eqs. (D3) and (D5). We conclude that the value of g_{pn} adopted in the calculation is physically justified.

APPENDIX E: BCS SOLUTIONS FOR NEUTRONS

For the sake of completeness, we present here the results of the conventional BCS calculation for neutrons (Tables XII and XIII). The single-particle states and the strength of the isovector coupling are explained in the text and in the previous appendices.

[1] J. D. Vergados, Phys. Rep. **361**, 1 (2002).
[2] H. Ejiri, Phys. Rep. **338**, 265 (2000).
[3] M. Doi and T. Kotani, Prog. Theor. Phys. **87**, 1207 (1992).
[4] F. T. Avignone III, S. R. Elliott, and J. Engel, Rev. Mod. Phys. **80**, 481 (2008).
[5] W. C. Haxton and G. J. Stephenson Jr., Prog. Part. Nucl. Phys. **12**, 409 (1984).
[6] E. Caurier, G. Martinez-Pinedo, F. Nowacki, A. Poves, and A. P. Zuker, Rev. Mod. Phys. **77**, 427 (2005).
[7] M. Kortelainen and J. Suhonen, Phys. Rev. C **75**, 051303(R) (2007).
[8] O. Civitarese and J. Suhonen, Nucl. Phys. **A761**, 313 (2005).
[9] V. A. Rodin, A. Faessler, F. Simkovic, and P. Vogel, Phys. Rev. C **68**, 044302 (2003); Nucl. Phys. **A766**, 107 (2006); Nucl. Phys. **A766**, 107(Erratum) (2006).
[10] D. Cha, Phys. Rev. C **27**, 2269 (1983).
[11] P. Vogel and M. R. Zirnbauer, Phys. Rev. Lett. **57**, 3148 (1986).
[12] O. Civitarese, A. Faessler, and T. Tomoda, Phys. Lett. **B194**, 11 (1987).
[13] E. Marshalek and J. Weneser, Ann. Phys. **53**, 569 (1969).
[14] D. R. Bes, G. G. Dussel, R. A. Broglia, R. J. Liotta, and B. R. Mottelson, Phys. Lett. **B52**, 253 (1974).
[15] D. R. Bes and J. Kurchan, *The Treatment of Collective Coordinates in Many Body Systems*, World Scientific Lecture Notes, Vol. 34 (World Scientific Publishing Company, Singapore, 1990).
[16] D. R. Bes, R. A. Broglia, G. G. Dussel, and R. J. Liotta, Phys. Lett. **B56**, 109 (1975).
[17] J. Suhonen and O. Civitarese, Phys. Rep. **300**, 123 (1998).
[18] D. R. Bes and O. Civitarese, Phys. Rev. C **78**, 014317 (2008).
[19] A. Bohr and B. R. Mottelson, *Nuclear Structure* (W. A. Benjamin, Inc., New York, Amsterdam, 1975), Vol. 1.
[20] V. Tretyak and Y. G. Zdesenko, At. Data Nucl. Data Tables **80**, 83 (2002).
[21] O. K. Manuel, J. Phys. G **17**, S221 (1991).
[22] T. Bernatowicz, J. Brannon, R. Brazzle, R. Cowsik, C. Hohenberg, and F. Podosek, Phys. Rev. C **47**, 806 (1993).
[23] H. Ohsumi, J. Phys. Conference Series **120**, 052047 (2008).
[24] A. Barabash, Czech. J. Phys. **56**, 437 (2006).
[25] L. Simard, AIP Conf. Proc. **942**, 72 (2008).
[26] Dieter Frekers (private communication).
[27] S. J. Freeman *et al.*, Phys. Rev. C **75**, 051301(R) (2007); J. P. Schiffer (private communication).
[28] J. Suhonen and O. Civitarese, Phys. Lett. **B668**, 277 (2008).
[29] K. Zuber, AIP Conf. Proc. **942**, 96 (2008).
[30] G. Audi and A. H. Wapstra, Nucl. Phys. **A595**, 409 (1995); G. Audi and C. Thibault, *ibid.* **A729**, 337 (2003).
[31] D. R. Bes and R. Broglia, in *Modi elementari di eccitazione nei nuclei*, edited by A. Bohr and R. A. Broglia (North Holland Publishing Co., Amsterdam, 1977), p. 55.
[32] H. W. Fielding, R. E. Anderson, C. D. Zafiratos, D. A. Lind, F. E. Cecil, and H. H. Wieman, Nucl. Phys. **A281**, 389 (1977).
[33] H. W. Fielding, R. E. Anderson, P. D. Kunz, D. A. Lind, and C. D. Zafiratos, Nucl. Phys. **A304**, 520 (1978).
[34] W. P. Alford, R. E. Anderson, P. A. Batay-Csorba, R. A. Emigh, D. A. Lind, P. A. Smith, and C. D. Zafiratos, Nucl. Phys. **A323**, 339 (1979).
[35] Nucl. Data Sheets 77, 1, 15; **4**, 645 (1996).
[36] A. Bohr and B. R. Motelson, *Nuclear Structure*, Vol. 2 (W. A. Benjamin, Inc., New York, Amsterdam, 1975).
[37] M. Baranger and K. Kumar, Nucl. Phys. **A110**, 490 (1968).
[38] D. R. Bes and R. A. Sorensen, *The Pairing plus Quadrupole Model.* Advances in Nuclear Physics (Plenum Press, New York, 1969), Vol. 2, p. 129.